

Iron-based heavy quasiparticles in SrFe₄Sb₁₂: An infrared spectroscopic study

Shin-ichi Kimura*

*UVSOR Facility, Institute for Molecular Science, Okazaki 444-8585, Japan
and School of Physical Sciences, The Graduate University for Advanced Studies (SOKENDAI), Okazaki 444-8585, Japan*

Takafumi Mizuno and Hojun Im

School of Physical Sciences, The Graduate University for Advanced Studies (SOKENDAI), Okazaki 444-8585, Japan

Katsuyuki Hayashi and Eiichi Matsuoka†

Department of Quantum Matter, ADSM, Hiroshima University, Higashi-Hiroshima 739-8530, Japan

Toshiro Takabatake

*Department of Quantum Matter, ADSM, Hiroshima University, Higashi-Hiroshima 739-8530, Japan
and Institute for Advanced Materials Research, Hiroshima University, Higashi-Hiroshima 739-8530, Japan*

(Received 10 April 2006; published 9 June 2006)

Temperature-dependent infrared reflectivity spectra of SrFe₄Sb₁₂ has been measured. A renormalized Drude peak with a heavy effective mass and a pronounced pseudogap of 10 meV develops in the optical conductivity spectra at low temperatures. As the temperature decreases below 100 K, the effective mass (m^*) rapidly increases, and the scattering rate ($1/\tau$) is quenched. The temperature dependence of m^* and $1/\tau$ indicates that the hybridization between the Fe 3d spins and the charge carriers plays an important role in determining the physical properties of SrFe₄Sb₁₂ at low temperatures. This result is the clear evidence of the iron-based heavy quasiparticles.

DOI: [10.1103/PhysRevB.73.214416](https://doi.org/10.1103/PhysRevB.73.214416)

PACS number(s): 75.50.Bb, 78.30.-j, 71.20.Lp, 74.25.Gz

I. INTRODUCTION

Recently, heavy quasiparticles or heavy fermions normally appearing in Ce- and Yb-based compounds have been observed in transition-metal compounds,¹ for example LiV₂O₄,² MnSi,³ and ZrZn₂,^{4,5} to name a few. These materials have attracted attention because of their various physical properties, including those related to their performance as unconventional superconductors.⁶ The origin of the various physical properties is believed to be related to the hybridization of charge carriers to localized spins. Alkaline-earth-filled iron-antimony skutterudites ($A^{2+}\text{Fe}_4\text{Sb}_{12}$), including the SrFe₄Sb₁₂ system studied in this paper, are almost ferromagnetic systems with a paramagnetic Curie temperature (T_C) of 53 K.⁷⁻⁹ Alkali-filled iron-antimony skutterudites ($A^+\text{Fe}_4\text{Sb}_{12}$) possess an itinerant ferromagnetic character with a $T_C=80$ K.¹⁰⁻¹² Both systems can be fundamentally explained by the self-consistent renormalization (SCR) theory.¹³ However, the Sommerfeld coefficient, γ , is enhanced by about 100 mJ/mol K² in $A^{2+}\text{Fe}_4\text{Sb}_{12}$ (Ref. 7) compared to 53.2 mJ/mol K² predicted by a band structure calculation.¹⁴ In addition, the ratio between the enhanced coefficient A of the quadratic electrical resistivity ($\rho=AT^2$) and γ is close to the Kadowaki-Woods value [$1.0 \times 10^{-5} \mu\Omega \text{ cm K}^{-2}/(\text{mJ/mol K}^2)^2$].⁷ This indicates that the hybridization between the charge carriers and the localized spins in $A^{2+}\text{Fe}_4\text{Sb}_{12}$ plays an important role at low temperatures. The physical properties of SrFe₄Sb₁₂ are similar to those of the transition-metal compounds mentioned above. Therefore, SrFe₄Sb₁₂ should exhibit similar physical properties to those of other transition-metal compounds as well as heavy fermion compounds.

The hybridization of the charge carriers to the localized magnetic moments forms heavy quasiparticles, which is called “Kondo effect.” In optical spectra, a renormalized Drude absorption due to these heavy quasiparticles is observed. In heavy fermions and other transition-metal compounds mentioned above, the enhancement in the optical conductivity [$\sigma(\omega)$] at $\hbar\omega=0$ eV (coherent peak) and a peak at higher energy (incoherent peak) increase at low temperatures despite the fact that Drude curves for metals usually appear at high temperatures. Such a change in $\sigma(\omega)$ has been observed in MnSi (Ref. 15) and Sr₂RuO₄ (Ref. 16) and in high- T_C cuprates.^{17,18} To clarify the appearance of the coherent and incoherent peaks in SrFe₄Sb₁₂ as well as the origin of the large γ , the temperature and magnetic field dependence of $\sigma(\omega)$ were measured and the effective mass (m^*) and scattering rate [$1/\tau$] were derived from the $\sigma(\omega)$ spectra.

$\sigma(\omega)$ in $A^{2+}\text{Fe}_4\text{Sb}_{12}$ ($A^{2+}=\text{Ca}, \text{Ba}$) was previously reported to determine the origin of the pseudogap structure in divalent YbFe₄Sb₁₂.¹⁹ Even though all of the 4f states are occupied in YbFe₄Sb₁₂, a pseudogap similar to the c - f hybridization gap that generally appears in heavy fermion materials was observed above 10 meV.²⁰ The paper *only* concluded that the origin of the pseudogap structure in YbFe₄Sb₁₂ was generated largely by the Fe 3d density of states. In addition, $\sigma(\omega)$ for this system roughly reflects the unoccupied electronic states of the Fe₄Sb₁₂ frame.^{14,21} However, the previous paper did not clarify the origin of the heavy-quasiparticle-like character appearing in the thermodynamical properties.⁷ In this communication, we point out the important role of the hybridization of carriers to the Fe 3d spins from the temperature and photon energy dependence of the effective mass and scattering rate of SrFe₄Sb₁₂

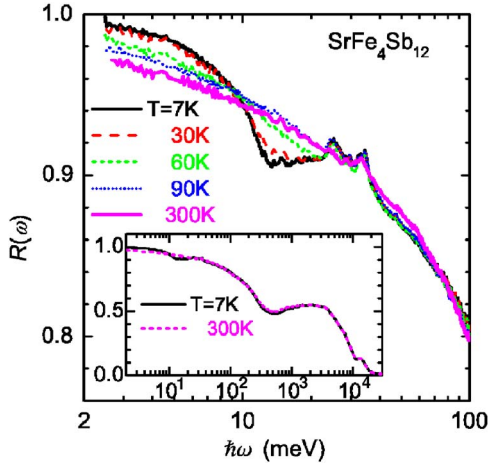


FIG. 1. (Color online) The temperature-dependent reflectivity spectrum $[R(\omega)]$ in the photon energy range of 2–100 meV. Inset, $R(\omega)$ at 7 and 300 K in the photon energy range of 2 meV–30 eV.

based on the temperature dependence of the $\sigma(\omega)$ spectrum *below* the pseudogap.

II. EXPERIMENT

A high-density polycrystalline $\text{SrFe}_4\text{Sb}_{12}$ sample was synthesized using a spark-plasma sintering technique previously reported.⁷ The near-normal incident optical reflectivity spectra $[R(\omega)]$ of $\text{SrFe}_4\text{Sb}_{12}$ were acquired from well polished samples by using 0.3 μm -grain-size Al_2O_3 wrapping film sheets. Martin-Puplett and Michelson type rapid-scan Fourier spectrometers were used at photon energies ($\hbar\omega$) of 2.5–30 meV and 5 meV–1.5 eV, respectively, at sample temperatures between 7–300 K. $R(\omega)$ under magnetic fields up to 6 T were also acquired by using a magneto-optical instrument at the beam line 6B of a synchrotron radiation ring, UVSOR-II, Institute for Molecular Science.²² To obtain $R(\omega)$, the sample was evaporated *in-situ* with gold. A reference spectrum was then measured. To obtain $\sigma(\omega)$ via the Kramers-Kronig analysis (KKA), $R(\omega)$ at 300 K with zero magnetic field was measured over the energy range of 1.2–30 eV at the beam line 7B of UVSOR-II.²³ Since $R(\omega)$ above 1.2 eV does not significantly change, even though the temperature and magnetic field change, the $R(\omega)$ above 1.2 eV was connected to $R(\omega)$ under various conditions in the energy range below 1.5 eV. In the energy ranges below 2.5 meV and above 30 eV, the spectra were extrapolated using the Hagen-Rubens function $[R(\omega)=1-(2\omega/\pi\sigma_{\text{DC}})^{1/2}]$ and $R(\omega)\propto\omega^{-4}$, respectively.²⁴ After constructing $R(\omega)$ in the energy region from zero to infinity, KKA was performed to obtain $\sigma(\omega)$.

III. RESULTS AND DISCUSSION

The temperature dependent $R(\omega)$ of $\text{SrFe}_4\text{Sb}_{12}$ obtained using the above method is shown in Fig. 1. $R(\omega)$ is a normal shape for a metal except for two significant peaks at 25 and 35 meV at the temperatures above 90 K. The spectra also

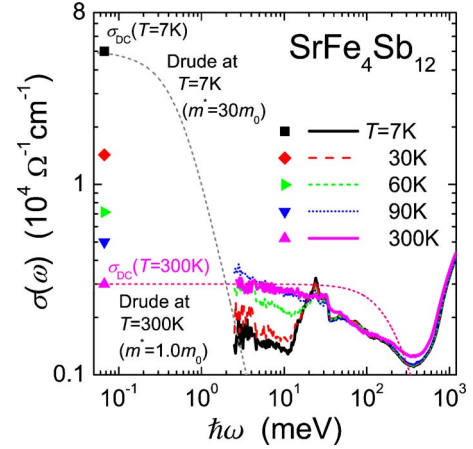


FIG. 2. (Color online) The temperature dependence of the optical conductivity spectrum $[\sigma(\omega)]$ of $\text{SrFe}_4\text{Sb}_{12}$ (solid lines) with the corresponding direct current conductivity (σ_{DC} , marks). The classical Drude curves at 7 and 300 K using the σ_{DC} , the carrier density derived from the Hall coefficient and the expected effective mass ($m^*/m_0=30$ for $T=7$ K and 1.0 for 300 K) are also shown.

show a dip at around 12 meV that gets more pronounced with decreasing temperature. Simultaneously, $R(\omega)$ below 10 meV increases to unity with decreasing temperature. These spectral changes are similar to those of heavy fermion compounds.^{25,26} The two peaks at 25 and 35 meV are not discussed in this paper because the peaks originate from optical phonons.¹⁹

The temperature dependence of $\sigma(\omega)$ derived from $R(\omega)$ and the direct current conductivities (σ_{DC}) at the corresponding temperatures are shown in Fig. 2. At 300 and 90 K, the extrapolation of $\sigma(\omega)$ to 0 eV is consistent with the σ_{DC} s, which is consistent with the $\sigma(\omega)$ of a normal metal. At 300 K, the Drude fitting curve with a single effective mass and single relaxation time (it is called the “classical Drude curve” hereafter) $[\sigma(\omega)=\sigma_{\text{DC}}/(1+\omega^2\tau^2)]$ roughly represents the experimental $\sigma(\omega)$ below 200 meV. Note that the upturn above 400 meV originates from the interband transition. Here, $\sigma_{\text{DC}}=N_{\text{eff}}e^2\tau/m_0$, where N_{eff} is the effective carrier density, τ is the relaxation time, and m_0 is the electron rest mass. N_{eff} relates to m^* with the function of $N_{\text{eff}}=N(m_0/m^*)$. The classical Drude curve at 300 K is calculated using the carrier density ($N=6.2\times 10^{20}\text{ cm}^{-3}$) obtained from the Hall coefficient²⁷ and m^* of $1.0m_0$ as evaluated by the *extended* Drude model analysis discussed later. With decreasing temperature, $\sigma(\omega)$ decreases at around 3 meV with a simultaneous increase in the σ_{DC} . The contradictory temperature dependence in $\sigma(\omega)$ and σ_{DC} indicates that m^* increases and $1/\tau$ decreases with decreasing temperature. It is noted that the classical Drude curve fitted at 7 K shown in Fig. 2 requires very heavy effective mass, for instance, $m^*=30m_0$. However, the classical Drude curve at 7 K does not represent any of the obtained $\sigma(\omega)$. This means that strong photon energy dependent m^* and $1/\tau$ are expected.

To clarify the temperature and photon energy dependences of m^* and $1/\tau$, we used the *extended* Drude model analysis using the real and imaginary parts of the dielectric function derived from the Kramers-Kronig analysis of

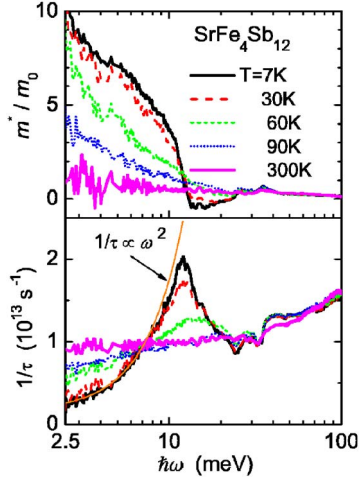


FIG. 3. (Color online) The temperature-dependent effective mass relative to the electron rest mass (m^*/m_0) and scattering rate ($1/\tau$) of $\text{SrFe}_4\text{Sb}_{12}$ as a function of photon energy. A $1/\tau \propto \omega^2$ relation is also plotted for comparison, and holds for $\hbar\omega < 8$ meV at temperatures below 30 K.

$R(\omega)$.^{17,28,29} The m^*/m_0 and $1/\tau$ are obtained from the following:

$$\frac{m^*}{m_0} = \frac{Ne^2}{m_0\omega} \text{Im}\left(\frac{1}{\tilde{\sigma}(\omega)}\right), \quad \frac{1}{\tau} = \frac{Ne^2}{m_0} \text{Re}\left(\frac{1}{\tilde{\sigma}(\omega)}\right).$$

Here, $\tilde{\sigma}(\omega)$ is the complex optical conductivity derived from KKA of the corresponding reflectivity spectrum. The m^*/m_0 and $1/\tau$ obtained from the analysis are plotted in Fig. 3. From the figure, both of m^* and $1/\tau$ are almost constant at 300 K, with values of about $1.0m_0$ and $1.0 \times 10^{13} \text{ s}^{-1}$ below 20 meV, respectively. This means that $\sigma(\omega)$ at 300 K can be described by the classical Drude model as shown in Fig. 2. With decreasing temperature, m^* below 10 meV monotonically increases from $(1.0 \pm 0.7) m_0$ at 300 K to $(9.0 \pm 0.3) m_0$ at 7 K at $\hbar\omega = 3$ meV. The behavior of $1/\tau$, however, is not as linear, with a peak at 12 meV increasing with decreasing temperature as well as a steeper decrease at lower energies, with a crossover point at about 6 meV. At 7 K, $1/\tau$ is proportional to ω^2 below 8 meV, indicating Fermi liquid behavior. These results indicate that heavy quasiparticles are generated at low temperatures.

Similar temperature and photon energy dependences have been observed in heavy fermions^{25,26} and high- T_C cuprates.^{17,18} In the case of $\text{SrFe}_4\text{Sb}_{12}$, $1/\tau$ has a peak at 12 meV, meaning carriers are scattered at that energy. The peak energy is lower than those of heavy fermions [40 meV in YbAl_3 ,²⁶ 17 meV in CePd_3 (Ref. 25)] and of Sr_2RuO_4 [20 meV (Ref. 16)]. This indicates that the lower-energy excitation is related to the creation of the heavy quasiparticles. An excitation energy of 12 meV corresponds to the energy gap of the “V”-shaped density of states originating from the hybridization band between the Fe 3d and Sb 5p states in the band structure calculation.^{14,21} Below the pseudogap, the hybridization between the charge carriers and the Fe 3d spins creates the heavy quasiparticles in $\text{SrFe}_4\text{Sb}_{12}$.

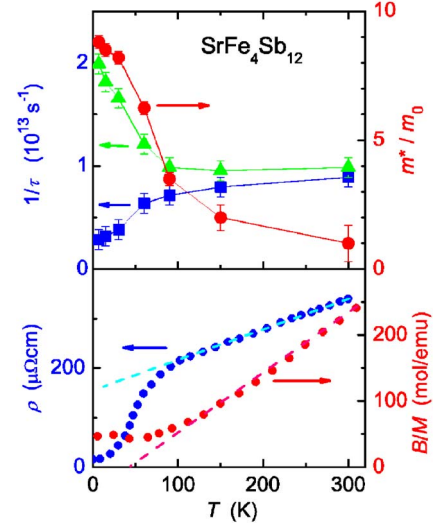


FIG. 4. (Color online) $1/\tau$ at 3 meV (solid square) and 12 meV (solid triangle) and m^*/m_0 (solid circle) as a function of temperature. The temperature dependence is compared with the electrical resistivity (ρ) and inverse magnetic susceptibility (B/M) (Ref. 7).

m^*/m_0 , $1/\tau$ at 3.0 meV, and $1/\tau$ at the peak energy of the scattering rate (12 meV) are plotted in Fig. 4 as a function of photon energy. The electrical resistivity (ρ) and the inverse magnetic susceptibility (B/M) (Ref. 7) are also plotted for comparison. As can be seen in Fig. 4, m^*/m_0 and $1/\tau$ dramatically change below 100 K. In particular, m^* at 7 K is about 9 times larger than that at 300 K. This enhancement of the effective mass is similar to the enhancement value of 8.7 of γ in $\text{SrFe}_4\text{Sb}_{12}$ compared with $\text{SrRu}_4\text{Sb}_{12}$ (10 mJ/mol K²).³⁰ The electronic structure near E_F of $\text{SrFe}_4\text{Sb}_{12}$ is similar to that of $\text{SrRu}_4\text{Sb}_{12}$ at 300 K because the $\sigma(\omega)$ of $\text{SrFe}_4\text{Sb}_{12}$ below 100 meV is the same as that of $\text{SrRu}_4\text{Sb}_{12}$ at 300 K.³¹ Therefore, the mass enhancement at low temperatures has the same origin as the enhancement in γ .³²

The temperature dependences of m^*/m_0 and $1/\tau$, which indicate the anomaly at around 100 K are consistent with ρ and B/M as shown in Fig. 4. According to the nuclear quadrupole resonance (NQR) result, the ferromagnetic spin fluctuation is dominant above 100 K.⁹ Below 100 K, $(1/T_1T)_{\text{spin}}$ drops from the line of $(1/T_1T)_{\text{spin}} \propto \chi_{\text{spin}}$, which cannot be explained by the SCR theory. This drop implies that the low-energy magnetic excitations associated with the spin fluctuations are almost inhibited at low temperatures. The optical results indicate that the suppression of the spin fluctuations and the creation of the heavy quasiparticles observed in $\sigma(\omega)$ are coincident, or in the other words, the origin of these phenomena is the hybridization between the Fe 3d spins and the charge carriers. This is consistent that the ratio between A of $\rho = AT^2$ and γ in $\text{SrFe}_4\text{Sb}_{12}$ is close to the Kadowaki-Woods value as pointed out before.⁷

If the mass enhancement that appears in $\sigma(\omega)$ originates from the hybridization of the charge carriers to the Fe 3d spins, the spectrum must change under magnetic fields. Figure 5(a) confirms this, as the peak in $\sigma(\omega)$ at around 20 meV decreases, and the dip below 12 meV disappears with in-

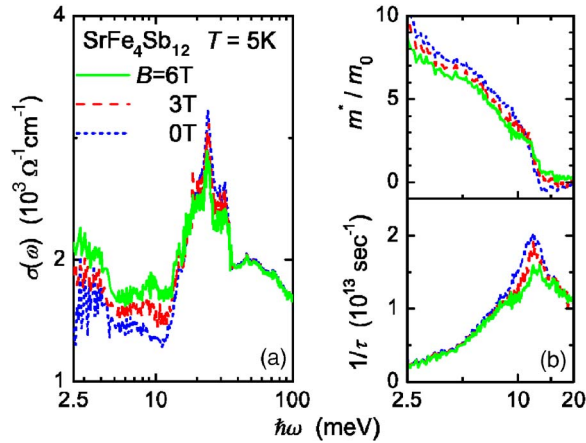


FIG. 5. (Color online) (a) The magnetic field dependence of $\sigma(\omega)$ of $\text{SrFe}_4\text{Sb}_{12}$ and (b) the magnetic field dependent effective mass relative to the electron rest mass (m^*/m_0) and scattering rate ($1/\tau$) as a function of photon energy.

creasing magnetic field strength. σ_{DC} also decreases with increasing magnetic field strength.⁸ The combination of the decreasing σ_{DC} and the change in $\sigma(\omega)$ implies that the coherent and incoherent peaks collapse in the presence of a magnetic field. The effective mass of the quasiparticles decreases with increasing magnetic field strength in spite that the scattering rate at the accessible lowest photon energy of 2.5 meV does not change as shown in Fig. 5(b). This is direct evidence of the creation of heavy quasiparticles due to the hybridization between charge carriers and the Fe 3*d* spins at low temperatures in $\text{SrFe}_4\text{Sb}_{12}$. The magnetic field dependent effective mass is similar to that of a Ce-based heavy fermion skutterudite, $\text{CeRu}_4\text{Sb}_{12}$.³³ The paper pointed out the effective mass as a function of magnetic field is suppressed as $1/B^2$. However, since our accessible maximum magnetic field is 6 T, unfortunately we cannot follow the magnetic field dependence of the effective mass. The optical measurement at higher magnetic fields for $\text{SrFe}_4\text{Sb}_{12}$ should be done for the complement.

In the above discussion, it is clear that the hybridization between the charge carriers and the Fe 3*d* spins is important in understanding the physical properties in $\text{SrFe}_4\text{Sb}_{12}$. However, no heavy quasiparticles appear in $A^+\text{Fe}_4\text{Sb}_{12}$ ($A^+ = \text{Na}, \text{K}$) because there is no coherent peak in $\sigma(\omega)$,³⁴ in spite

that $A^+\text{Fe}_4\text{Sb}_{12}$ possess an itinerant ferromagnetic character with a $T_C = 80$ K which is higher than that of $A^{2+}\text{Fe}_4\text{Sb}_{12}$. On the contrary, trivalent $\text{LaFe}_4\text{Sb}_{12}$ is an enhanced paramagnetic metal. The different physical character in $A\text{Fe}_4\text{Sb}_{12}$ originates in the difference in the carrier density due to the different valence number of guest atoms, i.e., $A^+\text{Fe}_4\text{Sb}_{12}$ has the highest carrier density and $\text{LaFe}_4\text{Sb}_{12}$ has the lowest based on the positive Hall coefficient.²⁷ The situation is similar to the carrier-density-controlled phase diagram in a heavy fermion system such as $\text{Ce}(\text{Ru}_{1-x}\text{Rh}_x)_2\text{Si}_2$.³⁵ In comparing $A\text{Fe}_4\text{Sb}_{12}$ with the phase diagram of $\text{Ce}(\text{Ru}_{1-x}\text{Rh}_x)_2\text{Si}_2$, $A^+\text{Fe}_4\text{Sb}_{12}$ and $\text{LaFe}_4\text{Sb}_{12}$ seem to be located in local and itinerant regimes compared to $A^{2+}\text{Fe}_4\text{Sb}_{12}$, respectively. Therefore, the unconventional physical properties observed in $A^{2+}\text{Fe}_4\text{Sb}_{12}$ are concluded to originate from the strong hybridization between the charge carriers and the Fe 3*d* spins.

IV. CONCLUSION

In conclusion, the temperature dependence of the optical conductivity of $\text{SrFe}_4\text{Sb}_{12}$ was measured in the photon energy range of 2.5 meV–30 eV. With decreasing temperature, clear signatures of heavy quasiparticle behavior are found. The optical effective mass is strongly enhanced below 10 meV and the scattering rate at 12 meV increases with decreasing temperature below 100 K. The temperature dependence is consistent with the suppression of the spin fluctuations of the Fe 3*d*. This indicates that the hybridization between the Fe 3*d* spins and charge carriers plays an important role in the creation of the heavy quasiparticles in $\text{SrFe}_4\text{Sb}_{12}$ and also in other $A^{2+}\text{Fe}_4\text{Sb}_{12}$ (Ref. 19) and $\text{YbFe}_4\text{Sb}_{12}$.²⁰

ACKNOWLEDGMENTS

The authors would like to thank K. Takegahara for fruitful discussion and Y. Sakurai for technical support for the reflectivity measurement in the VUV region. This work was a joint studies program of the Institute for Molecular Science (2005) and was partially supported by a Grant-in-Aids; the COE Research (13CE2002), the priority area ‘‘Skutterudite’’ (Grant No. 15072205) and Young Scientists (A) (Grant No. 14702011) from MEXT of Japan.

*Electronic address: kimura@ims.ac.jp

†Present address: Department of Physics, Tohoku University, Sendai, Japan

¹H.-A. Krug von Nidda, R. Bulla, N. Büttgen, M. Heinrich, and A. Loidl, *Eur. Phys. J. B* **34**, 399 (2003).

²S. Kondo, D. C. Johnston, C. A. Swenson, F. Borsa, A. V. Mahajan, L. L. Miller, T. Gu, A. I. Goldman, M. B. Maple, D. A. Gajewski, E. J. Freeman, N. R. Dilley, R. P. Dickey, J. Merrin, K. Kojima, G. M. Luke, Y. J. Uemura, O. Chmaissem, and J. D. Jorgensen, *Phys. Rev. Lett.* **78**, 3729 (1997).

³C. Pfleiderer, S. R. Julianand, and G. G. Lonzarich, *Nature (London)* **414**, 427 (2001).

⁴C. Pfleiderer, M. Uhlarz, S. M. Hayden, R. Vollmer, H. v. Löhneysen, N. R. Bernhoeftand, and G. G. Lonzarich, *Nature (London)* **412**, 58 (2001).

⁵S. J. C. Yates, G. Santi, S. M. Hayden, P. J. Meeson, and S. B. Dugdale, *Phys. Rev. Lett.* **90**, 057003 (2003).

⁶P. Coleman and A. J. Schofield, *Nature (London)* **433**, 226 (2005).

⁷E. Matsuoka, K. Hayashi, A. Ikeda, K. Tanaka, T. Takabatake,

- and M. Matsumura, J. Phys. Soc. Jpn. **74**, 1382 (2005).
- ⁸W. Schnelle, A. Leithe-Jasper, M. Schmidt, H. Rosner, H. Borrmann, U. Burkhardt, J. A. Mydosh, and Y. Grin, Phys. Rev. B **72**, 020402(R) (2005).
- ⁹M. Matsumura, G. Hyoudou, H. Kato, T. Nishioka, E. Matsuoka, H. Tou, T. Takabatake, and M. Sera, J. Phys. Soc. Jpn. **74**, 2205 (2005).
- ¹⁰A. Leithe-Jasper, W. Schnelle, H. Rosner, N. Senthilkumaran, A. Rabis, M. Baenitz, A. Gippius, E. Morozova, J. A. Mydosh, and Y. Grin, Phys. Rev. Lett. **91**, 037208 (2003).
- ¹¹A. Leithe-Jasper, W. Schnelle, H. Rosner, M. Baenitz, A. Rabis, A. A. Gippius, E. N. Morozova, H. Borrmann, U. Burkhardt, R. Ramlau, U. Schwarz, J. A. Mydosh, Y. Grin, V. Ksenofontov and S. Reiman, Phys. Rev. B **70**, 214418 (2004).
- ¹²G. Sheet, H. Rosner, S. Wirth, A. Leithe-Jasper, W. Schnelle, U. Burkhardt, J. A. Mydosh, P. Raychaudhuri, and Yu. Grin, Phys. Rev. B **72**, 180407(R) (2005).
- ¹³K. Ueda and T. Moriya, J. Phys. Soc. Jpn. **39**, 6687 (1975).
- ¹⁴K. Takegahara and H. Harima (unpublished).
- ¹⁵F. P. Mena, D. van der Marel, A. Damascelli, M. Fäth, A. A. Menovsky, and J. A. Mydosh, Phys. Rev. B **67**, 241101(R) (2003).
- ¹⁶T. Katsufuji, M. Kasai, and Y. Tokura, Phys. Rev. Lett. **76**, 126 (1996).
- ¹⁷A. V. Puchkov, D. V. Basov, and T. Timusk, J. Phys.: Condens. Matter **8**, 10049 (1996).
- ¹⁸S. V. Dordevic, C. C. Homes, J. J. Tu, T. Valla, M. Strongin, P. D. Johnson, G. D. Gu, and D. N. Basov, Phys. Rev. B **71**, 104529 (2005).
- ¹⁹J. Sichelschmidt, V. Voevodin, H. J. Im, S. Kimura, H. Rosner, A. Leithe-Jasper, W. Schnelle, U. Burkhardt, J. A. Mydosh, Yu. Grin, and F. Steglich, Phys. Rev. Lett. **96**, 037406 (2006).
- ²⁰S. V. Dordevic, D. N. Basov, N. R. Dilley, E. D. Bauer, and M. B. Maple, Phys. Rev. Lett. **86**, 684 (2001).
- ²¹S. Kimura, H. J. Im, Y. Sakurai, T. Mizuno, K. Takegahara, H. Harima, K. Hayashi, E. Matsuoka, and T. Takabatake, Physica B (to be published).
- ²²S. Kimura, Jpn. J. Appl. Phys., Suppl. **38**, 392 (1999).
- ²³K. Fukui, H. Miura, H. Nakagawa, I. Shimoyama, K. Nakagawa, H. Okamura, T. Nanba, M. Hasumoto, and T. Kinoshita, Nucl. Instrum. Methods Phys. Res. A **467-468**, 601 (2001).
- ²⁴F. Wooten, *Optical Properties of Solids* (Academic, New York, 1972).
- ²⁵B. C. Webb, A. J. Sievers, and T. Mihalisin, Phys. Rev. Lett. **57**, 1951 (1986).
- ²⁶H. Okamura, T. Michizawa, T. Nanba, and T. Ebihara, J. Phys. Soc. Jpn. **73**, 2045 (2004).
- ²⁷S. Morimoto *et al.* (unpublished).
- ²⁸S. I. Kimura, T. Nanba, S. Kunii, and T. Kasuya, Phys. Rev. B **50**, 1406 (1994).
- ²⁹J. W. Allen and J. C. Mikkelsen, Phys. Rev. B **15**, 2952 (1977).
- ³⁰E. Matsuoka, S. Narazu, K. Hayashi, K. Umeo, and T. Takabatake, J. Phys. Soc. Jpn. **75**, 014602 (2006).
- ³¹S. Kimura *et al.*, (unpublished).
- ³²Y. Takahashi, J. Phys.: Condens. Matter **13**, 6323 (2001).
- ³³S. V. Dordevic, K. S. D. Beach, N. Takeda, Y. J. Wang, M. B. Maple, and D. N. Basov, Phys. Rev. Lett. **96**, 017403 (2006).
- ³⁴J. Sichelschmidt *et al.* (unpublished).
- ³⁵T. Taniguchi, Y. Tabata, and Y. Miyako, J. Phys. Soc. Jpn. **68**, 2026 (1999).